Electrically evoked auditory steady state response detection in cochlear implant recipients using a system identification approach

Julian Schott*†, Robin Gransier†, Jan Wouters†, Marc Moonen*
*KU Leuven, Department of Electrical Engineering (ESAT),
STADIUS Center for Dynamical Systems, Signal Processing and Data Analytics, Belgium;
†KU Leuven, Department of Neurosciences, ExpORL, Belgium.
{julian.schott, robin.gransier, jan.wouters, marc.moonen}@kuleuven.be

***Abstract*—Regular Cochlear implant (CI) fitting is an important aspect of hearing restoration of CI recipients. CI stimulation parameters such as the so-called T- and C-levels are tuned to the recipient's needs and are crucial in hearing performance. Electrically evoked auditory steady state responses (EASSRs) are neural responses elicited by amplitude modulated stimulation pulse trains. They can be measured via electroencephalography (EEG) and have shown to be possible objective measures for CI fitting, which could lead to an automation of the fitting procedure and hence improve clinical care. However, artifacts in the EEG recording, originating from the CI stimulation, hamper EASSR detection. A number of stimulation artifact removal methods have been introduced and applied with different levels of success. EEG recordings with clinically relevant stimulation parameters, especially from ipsilateral recording channels, remain difficult to analyze. In this paper, we present a novel approach, which models EASSR and stimulation artifact using a system identification procedure. We use the apparent latency to compare its performance with that of the benchmark approach based on linear interpolation. The observed results suggest better stimulation artifact removal and EASSR detection with the new approach, especially for ipsilateral EEG recording channels.**

***Index Terms*—Cochlear implant, stimulation artifact, EASSR, objective, automatic**

I. Introduction

To this day, over 5% of the world's population (430 million) suffer from "disabling" hearing loss and require rehabilitation measures. It is estimated that by 2050 this number may even rise above 700 million people [1]. Cochlear implants (CI) have successfully been used to restore hearing in individuals, suffering from severe to profound hearing loss.

In a CI, the hearing sensation is recreated by electrically stimulating the auditory nerve with pulse trains, capturing the characteristics of sound or speech, recorded with an external microphone. The electrical stimulation occurs clinically between electrodes that are inserted into the cochlea and two extracochlear electrodes (monopolar (MP) stimulation mode), at typical pulse rates of 900pps and consists of biphasic, symmetric stimulation pulses [2].

An important part of CI rehabilitation is the recurring "fitting" of the implant. In these regular fitting sessions, starting a few weeks after implantation, the CI stimulation parameters are tuned to the subjective needs/characteristics of the recipient. Especially the so-called Threshold- and Comfort-levels, T- and C-levels respectively, which are the per electrode minimal and maximal current levels of the stimulation, are of great importance for hearing performance and require careful tuning. The fitting procedure is a time-consuming process where the outcome is highly dependent on the clinician that performs it and the feedback provided by the CI recipient. However, some CI recipients may not be able to respond appropriately (e.g., infants) or may be under anesthesia and hence not able to respond at all. Furthermore, the long duration of multiple fitting sessions with an audiologist and the need for highly trained experts often represent a bottleneck in the hearing restoration pipeline. Therefore, in order to provide reliable clinical care and enable fitting without necessary interaction with the CI recipient, objective measures need to be introduced.

Investigations with normal-hearing subjects have shown that auditory steady state responses, i.e., a neural response following the amplitude modulation (AM) of an acoustic stimulation pulse train, where the nerves "lock" their activity to the phase of the periodic acoustic stimuli (phase-locked response), can be used to objectively determine threshold levels which correlate well with the subjectively determined threshold levels [3]. Electrically evoked auditory steady state responses (EASSRs) could therefore be used to objectively determine stimulation levels in CI recipients [4] [5]. They are measured via electroencephalography (EEG) and their presence can be detected at the modulation frequency of the stimulus, using statistical methods such as F-test or Hotelling T^2 [6] [4]. The main challenge with detecting EASSRs are artifacts, originating from the CI stimulation pulses. They overlap with the desired response in time as well as frequency domain and can be several orders of magnitude larger than of the desired response [7]. These stimulation artifacts hinder the EASSR detection in the EEG, as they also have a component at the modulation frequency and may falsely be identified as EASSR, when solely analyzing the spectrum of the EEG. Signal processing methods to remove the stimulation artifacts are therefore required to correctly identify the presence of EASSRs.

In the past, different stimulation artifact removal methods for EASSR detection have been introduced and used in prac-

This work was funded by Cochlear Technology Centre Belgium and the Flanders Innovation & Entrepreneurship Agency through the VLAIO research Grant HBC.2019.2373. This work was partly funded by a Wellcome Trust Collaborative Award in Science RG91976 to Robert P. Carlyon, John C. Middlebrooks, and Jan Wouters. The authors thank E. Verwaerde for data collection and permission to use it.

tice with different levels of success. Linear interpolation (LI) as introduced in [8] is the most commonly used method in practice [4] [5] [8] [9] [10] [11]. As the artifact is time-locked to the stimulus pulses and decays with increasing distance to the pulses, the signal samples that are furthest away from the previous and closest to the following pulse are possibly free of artifact. These samples are retained from the original recording and the remaining ones in between are either removed (set to zero) or linearly interpolated. LI has shown good results for recordings, where the stimulation artifact duration is shorter than the inter-pulse interval. It therefore often works reliably for EASSRs elicited with lower stimulation rates (e.g., 500pps) and for contralateral EEG recordings [7]. Recent results have also shown success for recordings with clinically relevant stimulation rates (900pps), but only for contralateral recording channels [9].

Other stimulation artifact removal methods include template subtraction and spatial filtering approaches. Template subtraction requires an additional EEG recording to construct stimulation artifact templates, which are subsequently subtracted from the actual EEG recordings. Although promising results could be achieved even with clinically relevant stimulation rates [12], the necessity of an additional EEG recording is a major disadvantage for clinical implementation. Spatial filtering approaches such as independent component analysis are widely used in artifact removal in EEG, e.g., for transient CI responses such as CAEPs, EABR and ECAP ([13] [14] [15]) and also for EASSRs [16] [17]. The results for EASSR detection are mixed, as the nature of the stimulation artifact does not allow perfect determination of independent components. Rejection of artifact components may then lead to undesired removal of neural response [16].

All aforementioned methods perform the final EASSR detection in the frequency domain by checking the amplitude and phase at the modulation frequency. One method, that lays the foundation for the new approach that we present here, performs EASSR detection in the time domain. In [18] the separation of stimulation artifact and EASSR is formulated as a system identification problem, which is solved via state estimation with Kalman filtering. Here, the EEG recording is assumed to be a linear combination of stimulation artifact and EASSR. By fitting an artifact and neural response model to the recorded data, the estimated model parameters can be used to identify the EASSR and separate it from the stimulation artifact. In [18] the approach was only applied to clinically less relevant CI stimulation rates and the artifact model was much simplified and is hence not generally applicable to all EASSR recordings.

In this paper, we formulate a generalized system model, where both the EASSR and the stimulation artifact are fully estimated from the recordings. This allows wide application without any a priori assumptions of expected stimulation artifact shape. We apply the new EASSR detection approach to one clinically relevant pilot dataset and compare its results to that of LI. Preliminary results are presented and discussed.

II. Materials and Methods

A. Dataset

EEG recordings were collected for one adult CI recipient, implanted to the left side. Stimuli were generated using custom software and directly delivered to the implant using the NIC4 research interface platform (Cochlear Ltd.). The AM pulse trains consisted of symmetric biphasic cathodic-first pulses, with equal phase width of $25\mu s$ and interphase gap of $8\mu s$ and were presented at pulse rates of 900pps between intracochlear electrode 15 and extracochlear MP1+2 (MP mode). Stimulations with modulation frequencies of 37, 40 and 43Hz were used with a modulation depth of 50 current levels (CL) between an a priori determined C-level and C-50 CL.

A Biosemi ActiveTwo Hyper-Rate EEG recording system with sampling rate of 262.144kHz was used to perform the 8-channel recordings. Six recording electrodes were placed according to the international 10-20 system at $P9$, $P10$, Iz, Cz, Fz, Fpz and two extra electrodes at the left and right mastoid respectively (MaL, MaR). A signal of approximately 5 minutes per modulation frequency was recorded.

The EEG signals were low-pass filtered with the system's built-in analog third-order antialiasing filter having a -3 dB point at 50 kHz. Off-line referencing with Cz was performed and detrending with a second-order polynomial was applied. The signals were then, based on the stimulation triggers, split into epochs of 1.024s duration and 5% of the epochs with the highest peak-to-peak amplitudes were rejected. The mean epoch for MaR, MaL, $P9$, $P10$ and Iz was used for the further analysis.

B. Method

1) Apparent latency: In order to reliably detect EASSRs, even in the presence of residual stimulation artifact, the apparent latency is determined from a range of recordings with different modulation frequencies [3] [5] [4]. Latency values around 35-55ms are to be expected for EASSRs elicited from modulation frequencies around 40Hz, whereas latencies of 0ms indicate that residual stimulation artifact is present [19] [20]. The apparent latency is technically the equivalent to the group delay of the stimulated/measured system. EASSRs can therefore be detected by identifying the transfer function of a finite impulse response (FIR) system as introduced in the following section.

2) System model: Fig. 1 depicts the block diagram of the modelled EEG recording. The upper system (FIR1) represents the EASSR, of which the group delay is to be determined. The input $m[k]$ is the modulating component of the stimulus at discrete time k as defined in (3). This system is assumed to have a linear phase response in the range of the used input modulations. The output $r[k]$ is the EASSR to be identified.

The lower system (FIR2) represents the stimulation artifact. The input $u[k]$ of the system represents the stimulus pulse train as defined in (8) and the output $a[k]$ represents the estimated stimulation artifact.

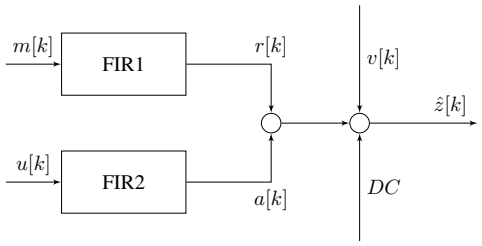

Fig. 1. Block diagram of modelled EASSR recording

The sum of stimulation artifact, EASSR, a DC component, to compensate for offset and drift, and additive noise $v[k]$ result in a model $\hat{z}$ for the actual EEG recording z.

$$\hat{z}[k] = r[k] + a[k] + DC + v[k]. \tag{1}$$

Following the diagram in Fig. 1, the EASSR is modeled as

$$\begin{aligned} r[k] =& \mathbf{M_k} \cdot \mathbf{b_{resp}} \\ =& \begin{bmatrix} m[k] & m[k-1q] & \dots & m[k-Mq] \end{bmatrix} \cdot \mathbf{b_{resp}} \end{aligned} \tag{2}$$

with the modulation component of the stimulus being

$$m[k] = \sin(2\pi f_m k T_s + \frac{\pi}{2}). \tag{3}$$

Here, f_m denotes the modulation frequency and $T_s = \frac{1}{F_s}$ is the sampling interval of the EEG recording system. Elements of $\mathbf{M_k}$ are shifted/downsampled by q samples, as especially the particularly high sampling rate of the used recording system, may otherwise lead to identifiability issues. When setting up the system of equations as in (12), the columns, corresponding to the shifted inputs, may be close to linearly dependent, hence a shift with $q > 1$ is used to decrease the condition number of the regressor matrix.

The phase shift θ and amplitude A of the EASSR are then determined via the transfer function of FIR1 evaluated at the modulation frequency f_m

$$\begin{aligned} &FIR1(z = e^{j2\pi f_m}) = \\ &\begin{bmatrix} 1 & e^{-jq2\pi f_m} & e^{-j2q2\pi f_m} & \dots & e^{-jMq2\pi f_m} \end{bmatrix} \cdot \mathbf{b_{resp}} \end{aligned} \tag{4}$$

$$A(f_m) = |FIR1(z = e^{j2\pi f_m})| \tag{5}$$

$$\theta(f_m) = \angle FIR1(z = e^{j2\pi f_m}). \tag{6}$$

The stimulation artifact is modeled similarly as

$$\begin{aligned} a[k] =& \mathbf{U_k} \cdot \mathbf{b_{arti}} \\ =& \begin{bmatrix} u[k] & u[k-1] & \dots & u[k-N] \end{bmatrix} \cdot \mathbf{b_{arti}}. \end{aligned} \tag{7}$$

Here, $u[k]$ models the AM-stimulus with parameters A_c and M determined by the subject-specific C-level

$$u[k] = A_c \cdot (1 + M \cdot m[k]) \cdot s[k] \tag{8}$$

$$A_c = \frac{C + (C - 50)}{2} \tag{9}$$

$$M = \frac{C - (C - 50))}{C + (C - 50))}. \tag{10}$$

One important aspect of this model is that unlike the actual physical stimulation with biphasic cathodic-first pulses, $s[k]$ is defined here as monophasic pulse train, with one sample per stimulation pulse, at a pulse rate of f_c.

$$s[k] = \begin{cases} 1, & \text{for } mod(kT_s, \frac{1}{f_c}) < T_s \\ 0, & \text{otherwise} \end{cases}. \tag{11}$$

This is due to the fact, that the biphasic pulse train itself does not have a component at f_m. However, non-linearities of the system introduce an asymmetry in the sampled pulses, which effectively leads to the artifact component at the modulation frequency [7]. As we are using a linear model, the input $u[k]$ requires a component at f_m, which is introduced through the monophasic $s[k]$.

The combined model for all $K + 1$ sampling points k is given in matrix-vector notation as

$$\hat{\mathbf{z}} = \underbrace{\begin{bmatrix} \mathbf{M} & \mathbf{U} & \mathbf{1} \end{bmatrix}}_{\mathbf{H}} \cdot \underbrace{\begin{bmatrix} \mathbf{b_{resp}} \\ \mathbf{b_{arti}} \\ x_{DC} \end{bmatrix}}_{\mathbf{x}} + \mathbf{v} \tag{12}$$

with $\hat{\mathbf{z}} = \begin{bmatrix} \hat{z}[0] & \hat{z}[1] & \dots & \hat{z}[K] \end{bmatrix}^\intercal$ and other quantities similarly defined. The DC component is added in form of a column vector of ones and scaled by x_{DC}.

As described, in order to calculate the apparent latency, at least two recordings with distinct modulation frequencies are required. The introduced system model in (12) allows combining these, as done in (13) for the three recordings of this study.

$$\hat{\mathbf{z}} = \begin{bmatrix} \hat{\mathbf{z}}^{37} \\ \hat{\mathbf{z}}^{40} \\ \hat{\mathbf{z}}^{43} \end{bmatrix}, \mathbf{H} = \begin{bmatrix} \mathbf{M^{37}} & \mathbf{U^{37}} & \mathbf{1} \\ \mathbf{M^{40}} & \mathbf{U^{40}} & \mathbf{1} \\ \mathbf{M^{43}} & \mathbf{U^{43}} & \mathbf{1} \end{bmatrix} \tag{13}$$

with superscripts referring to the modulation frequencies. This provides an advantage in identifying and disentangling EASSR and stimulation artifact, compared to all other artifact removal methods, where each recording is analyzed individually.

3) Kalman filtering: As in [18] we use Kalman filtering (KF) to determine $\mathbf{x}$. This approach can be of advantage, as it may deal with possible system dynamics, such as change in attention of the subject or adaption in the auditory pathway. The KF produces then for every sample an updated optimal solution for the coefficients.

The state-space model of the KF is given as

$$\begin{aligned} \mathbf{x_{k+1}} &= \mathbf{F_k x_k} + \mathbf{w_k} \\ z_k &= \mathbf{H_k x_k} + v[k] \end{aligned} \tag{14}$$

where $\mathbf{H_k}$ is the k-th row of $\mathbf{H}$. The unknown state vector $\mathbf{x_k}$ at discrete time index k consists of the coefficients as introduced in (12) and may vary over time according to the state transition matrix $\mathbf{F_k}$. As the system dynamics are unknown and no assumptions about them can be made, the state vector is assumed to follow a random walk model and

is subject to process noise $\mathbf{w_k}$, which is assumed to be zero-mean Gaussian white noise with covariance matrix $\mathbf{Q_k}$, i.e.,

$$\mathbf{F_k} = \mathbf{I_{N+M+3}} \tag{15}$$

and

$$\mathbf{Q_k} = diag(q_{resp0}, q_{resp1}, ..., q_{respM}, q_{arti0}, ..., q_{artiN}, q_{DC}). \tag{16}$$

Here, q_{resp}, q_{arti} and q_{DC} represent the assumed variances for the EASSR, stimulation artifact and DC states respectively and can be seen as tuning parameters of the algorithm. Lower values allow smoother but slower convergence of the states and may lead to more stable results. Higher values allow faster updates and hence more responsiveness to the system dynamics but less reliable convergence. Due to higher uncertainties and faster dynamics in the stimulation artifact, the variances q_{arti} are tuned to be larger than q_{resp} to allow faster responsiveness.

In order to reduce the complexity of the system model, recording samples, occurring close to the CI stimulation pulses are removed/skipped. This reduces processing time and avoids non-linearities, which are assumed to be present around the stimulation pulse.

4) Parameter tuning: The results presented in this paper were achieved with system model and KF parameters as shown in TABLE I.

III. Results and Discussion

Fig. 2 shows the determined latencies from LI and the newly introduced approach, applied to the mean epoch signal of the selected recording electrode. One-sample Hotelling T^2 was applied to determine if the estimated EASSR per modulation frequency differed significantly from the background activity. A significance level of 5% was used and when the p-value of at least one recording exceeded this level, the determined latency was deemed non-significant, indicated by reduced opacity and a red frame around the plot point. These results are ignored during box-plot creation and only drawn for completeness.

The first box, indicated with LI_500, shows the results for LI, with a short interpolation between $100\mu s$ before and $400\mu s$ after the stimulation pulse. It is clearly seen that the short interpolation is only sufficient for electrode I_z, as only here the determined apparent latency is in the expected range. The remaining electrode signals after LI are still dominated by the stimulation artifact, seen by the low apparent latency values, flat phase responses in Fig. 3 and higher amplitudes at modulation frequencies as shown in Fig. 4.

TABLE I
Required parameter settings for system model creation and Kalman Filter tuning.

Parameter	Description	Value
M	Order of FIR1	4
N	Order of FIR2	370
q	Shift in EASSR model	724
Skipping interval	Skipped observation samples	From $100\mu s$ before to $450\mu s$ after pulse
$q_{resp0-M}$	Response state variance	1e-10
$q_{arti0-N}$	Artifact state variance	1e-6
q_{DC}	DC state variance	1e-6
R_k	Observation noise variance	Recording noise level
$\mathbf{x_0}$	Initial state estimates	$\mathbf{0}$
$\mathbf{P_0}$	Initial error covariance	$1e5 \cdot \mathbf{I}$

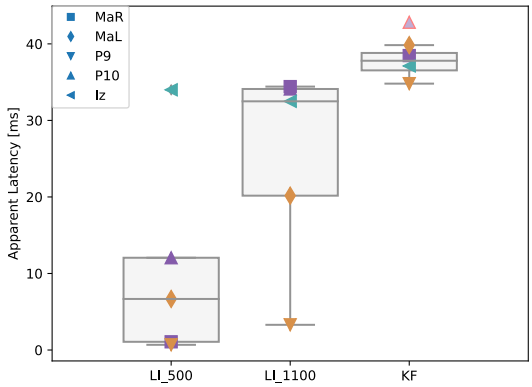

Fig. 2. Apparent latency values as determined by different EASSR detection methods. Ipsilateral ■ contralateral ■ and central ■ electrodes. Non-significant results with less opacity and red frame.

The results for LI with a long interpolation between $100\mu s$ before and $1000\mu s$ after the stimulation pulse are shown in box LI_1100. The increase of the interpolation length from $500\mu s$ to $1100\mu s$ leads to sufficient artifact removal in the contralateral electrodes MaR and $P10$. However, the determined latencies for ipsilateral electrodes MaL and $P9$ remain low after LI. With an interpolation length of $1.1ms$ and inter-pulse interval of $T_p = \frac{1}{900} = 1.11ms$, it becomes evident that the stimulation artifact exceeds the inter-pulse interval in the ipsilateral recordings and can hence not fully be removed via LI.

As the KF produces a state or coefficient estimate $\mathbf{x}$ respectively for every discrete time index k, a phase shift and amplitude, as described in (4) - (6), can be calculated for every k. To ensure good convergence, the average of the last 5% of the estimated state values are used to calculate the phase response and hence apparent latency of the EASSR. The resulting values indicate that for all recording electrodes, the stimulation artifact could sufficiently be removed. The phase responses in Fig. 3 are linear and very similar for all recording electrodes. $P10$ is deemed non-significant due to the recording with f_m = 43Hz, as seen in Fig. 3 and 4. However, this may result from the specific significance testing for KF, where for every iteration step a p-value can be calculated. When more than 10% of all calculated p-values are above the defined significant level of 5%, the recording is deemed non-significant. However, this is mostly the case for small k, when the estimate has not converged yet. The estimated phases and amplitudes for $P10$ (Fig. 3 and Fig. 4) are similar to those of the other recording electrodes, which may suggest correct estimation also for $P10$. When compared to LI_500 with an interpolation length similar to the number of skipped samples used with KF, it is clear that the majority of stimulation

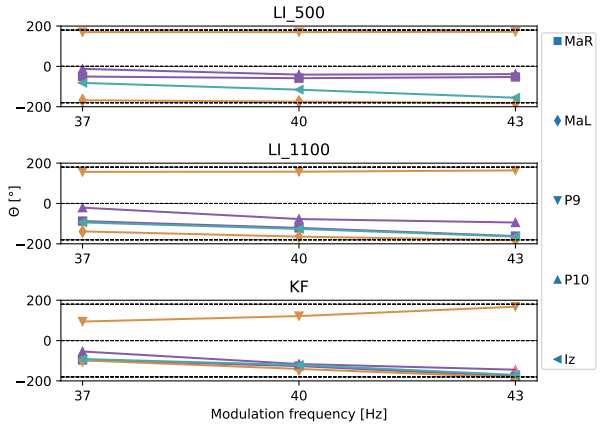

Fig. 3. Phase shift per modulation frequency as determined by different EASSR detection methods. 0°, 180° and −180° indicated by dashed horizontal lines.

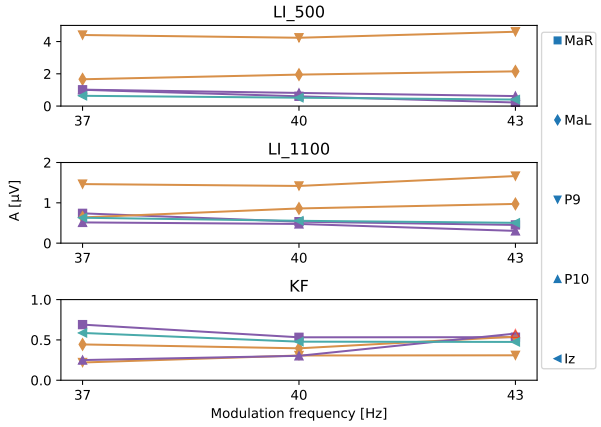

Fig. 4. EASSR amplitude per modulation frequency as determined by different EASSR detection methods.

artifact removal stems from the modelling of FIR2 and not the skipping of samples.

IV. Conclusion

In this paper a new approach to CI stimulation artifact removal and EASSR detection has been presented. It aims to identify the EASSR and stimulation artifact separately which allows separation in the EEG recording. The identification of the systems via finite impulse response estimation allows generalization without any a priori assumptions of the stimulation artifact shape as in [18]. Preliminary results show that the approach is applicable for clinically relevant stimulation rates in MP mode and can even remove stimulation artifacts that are longer than the inter-pulse interval. This would make it the first method in the field, which is major step towards objective and hence automatic fitting of CI recipients. Further validation with more subject data needs to be performed to confirm the results. Furthermore, future research should focus on how this approach performs for lower stimulation levels.

References

[1] World Health Organization, "Deafness and hearing loss," 2021. [Online]. Available: https://www.who.int/news-room/fact-sheets/detail/deafness-and-hearing-loss

[2] J. Wouters, H. J. McDermott, and T. Francart, "Sound coding in cochlear implants: From electric pulses to hearing," *IEEE Signal Processing Magazine*, vol. 32, no. 2, pp. 67–80, 2015.

[3] T. W. Picton, M. S. John, A. Dimitrijevic, and D. Purcell, "Human auditory steady-state responses: Respuestas auditivas de estado estable en humanos," *International Journal of Audiology*, 2003.

[4] M. Hofmann and J. Wouters, "Improved electrically evoked auditory steady-state response thresholds in humans," *JARO - Journal of the Association for Research in Otolaryngology*, 2012.

[5] R. Gransier, H. Deprez, M. Hofmann, M. Moonen, A. van Wieringen, and J. Wouters, "Auditory steady-state responses in cochlear implant users: Effect of modulation frequency and stimulation artifacts," *Hearing Research*, 2016.

[6] R. A. Dobie and M. J. Wilson, "A comparison of t test, F test, and coherence methods of detecting steady-state auditory-evoked potentials, distortion-product otoacoustic emissions, or other sinusoids," *The Journal of the Acoustical Society of America*, 1996.

[7] H. Deprez, R. Gransier, M. Hofmann, A. van Wieringen, J. Wouters, and M. Moonen, "Characterization of cochlear implant artifacts in electrically evoked auditory steady-state responses," *Biomedical Signal Processing and Control*, 2017.

[8] M. Hofmann and J. Wouters, "Electrically evoked auditory steady state responses in cochlear implant users," *JARO - Journal of the Association for Research in Otolaryngology*, 2010.

[9] R. Gransier, R. P. Carlyon, and J. Wouters, "Electrophysiological assessment of temporal envelope processing in cochlear implant users," *Scientific Reports*, vol. 10, no. 1, p. 15406, 2020. [Online]. Available: https://doi.org/10.1038/s41598-020-72235-9

[10] R. Gransier, R. Luke, A. Van Wieringen, and J. Wouters, "Neural Modulation Transmission Is a Marker for Speech Perception in Noise in Cochlear Implant Users," *Ear and Hearing*, 2020.

[11] A. Bahmer, S. Pieper, and U. Baumann, "Evaluation of an artifact reduction strategy for electrically evoked auditory steady-state responses: Simulations and measurements," *Journal of Neuroscience Methods*, vol. 296, pp. 57–68, 2018. [Online]. Available: http://dx.doi.org/10.1016/j.jneumeth.2017.12.025

[12] H. Deprez, R. Gransier, M. Hofmann, A. Van Wieringen, J. Wouters, and M. Moonen, "Template Subtraction to Remove CI Stimulation Artifacts in Auditory Steady-State Responses in CI Subjects," *IEEE Transactions on Neural Systems and Rehabilitation Engineering*, 2017.

[13] P. M. Gilley, A. Sharma, M. Dorman, C. C. Finley, A. S. Panch, and K. Martin, "Minimization of cochlear implant stimulus artifact in cortical auditory evoked potentials," *Clinical Neurophysiology*, 2006.

[14] N. Castañeda-Villa and C. J. James, "Independent component analysis for auditory evoked potentials and cochlear implant artifact estimation," *IEEE Transactions on Biomedical Engineering*, 2011.

[15] F. C. Viola, M. De Vos, J. Hine, P. Sandmann, S. Bleeck, J. Eyles, and S. Debener, "Semi-automatic attenuation of cochlear implant artifacts for the evaluation of late auditory evoked potentials," *Hearing Research*, 2012.

[16] H. Deprez, R. Gransier, M. Hofmann, A. Van Wieringen, J. Wouters, and M. Moonen, "Independent component analysis for cochlear implant artifacts attenuation from electrically evoked auditory steady-state response measurements," *Journal of Neural Engineering*, 2018.

[17] J. A. Undurraga, L. Van Yper, M. Bance, D. McAlpine, and D. Vickers, "Characterizing Cochlear implant artefact removal from EEG recordings using a real human model," *MethodsX*, vol. 8, p. 101369, 2021. [Online]. Available: https://doi.org/10.1016/j.mex.2021.101369

[18] R. Luke and J. Wouters, "Kalman filter based estimation of auditory steady state response parameters," *IEEE Transactions on Neural Systems and Rehabilitation Engineering*, 2017.

[19] R. Gransier, M. Hofmann, A. van Wieringen, and J. Wouters, "Stimulus-evoked phase-locked activity along the human auditory pathway strongly varies across individuals," *Scientific Reports*, 2021.

[20] R. Gransier, A. van Wieringen, and J. Wouters, "Binaural Interaction Effects of 30-50 Hz Auditory Steady State Responses," *Ear and hearing*, 2017.